

# UC Berkeley

## UC Berkeley Previously Published Works

### Title

Ni and CoO spin cantings induced by Fe layer in Ni/CoO/Fe/vicinal MgO(001)

### Permalink

<https://escholarship.org/uc/item/2jn6w45j>

### Journal

Physical Review B, 96(21)

### ISSN

2469-9950

### Authors

Li, Q  
Yang, M  
N'Diaye, AT  
[et al.](#)

### Publication Date

2017-12-01

### DOI

10.1103/physrevb.96.214405

Peer reviewed

**Ni and CoO spin cantings induced by Fe layer in Ni/CoO/Fe/vicinal MgO(001)**Q. Li,<sup>1</sup> M. Yang,<sup>1</sup> A. T. N'Diaye,<sup>2</sup> Q. Y. Dong,<sup>1</sup> A. Scholl,<sup>2</sup> A. T. Young,<sup>2</sup> N. Gao,<sup>1</sup> E. Arenholz,<sup>2</sup> C. Hwang,<sup>3</sup>  
J. Li,<sup>4,\*</sup> and Z. Q. Qiu<sup>1,†</sup><sup>1</sup>*Department of Physics, University of California at Berkeley, Berkeley, California 94720, USA*<sup>2</sup>*Advanced Light Source, Lawrence Berkeley National Laboratory, Berkeley, California 94720, USA*<sup>3</sup>*Korea Research Institute of Standards and Science, Yuseong, Daejeon 305-340, Korea*<sup>4</sup>*International Center for Quantum Materials and School of Physics, Peking University, Beijing 100871, China*

(Received 9 August 2017; revised manuscript received 24 October 2017; published 4 December 2017)

Using element-resolved x-ray magnetic circular dichroism and x-ray magnetic linear dichroism measurements, we studied Ni/CoO/vicinal MgO(001) and Ni/CoO/Fe/vicinal MgO(001) systems at 350 and 78 K. Above the CoO Néel temperature, the Ni magnetization is fully in plane and parallel to the atomic steps in both systems due to step-induced magnetic anisotropy. Below the CoO Néel temperature, the CoO spins in Ni/CoO/vicinal MgO(001) are fully in plane and parallel to the atomic steps and the Ni magnetization is fully in plane and perpendicular to the atomic steps due to the 90° Ni/CoO magnetic coupling. The CoO spins in Ni/CoO/Fe/vicinal MgO(001), however, develop an out-of-plane canted spin component in addition to the in-plane component parallel to the atomic steps. Consequently, the Ni magnetization is canted towards the out-of-plane direction by an appreciable angle. Photoemission electron microscopy imaging shows a 90° interfacial magnetic coupling at both the Ni/CoO and the CoO/Fe interfaces and an absence of a direct interlayer coupling, showing that the Ni spin canting is due to its coupling to the canted CoO spin components which is caused by the underlying ferromagnetic Fe layer in Ni/CoO/Fe/vicinal MgO(001).

DOI: [10.1103/PhysRevB.96.214405](https://doi.org/10.1103/PhysRevB.96.214405)**I. INTRODUCTION**

One important topic in nanomagnetism research is the controlling of spin orientation in magnetic thin films, especially the out-of-plane spin orientation, because the magnetic shape anisotropy favors an in-plane spin direction in a magnetic thin film. Magnetocrystalline anisotropy, which originates from the spin-orbit interaction [1], has been employed to generate an out-of-plane spin orientation. Since magnetocrystalline anisotropy depends on the lattice symmetry breaking, early realization of perpendicular magnetization was achieved by either the interfacial [2–5] or magnetostrictive symmetry breaking along the normal direction of the thin films [6]. Such lattice symmetry breaking permits the existence of a uniaxial magnetocrystalline anisotropy which is forbidden in bulk materials with cubic symmetry. Similarly, vicinal surfaces were later employed to break the in-plane rotation symmetry to generate an in-plane uniaxial magnetic anisotropy [7,8].

Parallel to the magnetocrystalline anisotropy, interfacial coupling between ferromagnetic (FM) and antiferromagnetic (AFM) materials was found to modify the spin orientation of the FM layer. In addition to the well-known exchange bias effect [9,10], the FM/AFM interaction is usually equivalent to an addition of various types of magnetic anisotropies to the FM layer [11], offering a new pathway to modify the FM layer magnetic properties. For example, it is found that a FM on top of an AFM layer could modify the FM layer perpendicular magnetic anisotropy, leading to a shift of the spin reorientation transition thickness [12,13]. Then it is obvious that the AFM spin configurations and spin states are important to the final magnetic anisotropies in the FM layer. For example,

the rotatable and frozen AFM spins in CoO could lead to very different magnetic anisotropies in the Fe film in the Fe/CoO system [14,15]. The winding/unwinding of a spiral domain wall in NiO film could lead to a uniaxial magnetic anisotropy in the FM overlayer [16]. An even more interesting phenomenon is that in a FM/AFM/FM sandwich, it is found that the two FM layers could behave very differently for different cooling histories due to different AFM spin configurations [17]. Then the interesting question is whether the AFM/FM interaction by one FM layer can modify significantly the magnetic anisotropy of another FM layer in a FM/AFM/FM sandwich. In this paper, we report a study of Ni/CoO/Fe grown on vicinal MgO(001) in which the CoO/Fe forms single-crystalline bilayer films. By comparing the Ni/CoO/vicinal MgO(001) and Ni/CoO/Fe/vicinal MgO(001) systems, we revealed the effect of the CoO/Fe interaction on the magnetic anisotropy of the Ni film. Element-resolved x-ray magnetic circular dichroism (XMCD) and x-ray magnetic linear dichroism (XMLD) measurements were utilized to determine the Ni, CoO, and Fe spin orientations separately. We find that the insertion of the Fe layer results in a CoO spin configuration different from the Ni/CoO bilayer system, and consequently leads to a Ni spin canting towards the out-of-plane direction in the Ni/CoO/Fe trilayers whereas the Ni spin in Ni/CoO bilayers is fully in the film plane.

**II. EXPERIMENT**

Ni/CoO and Ni/CoO/Fe films were prepared by molecular beam epitaxy (MBE) in an ultrahigh-vacuum (UHV) system. A vicinal MgO(001) substrate (7° vicinal angle with steps parallel to the  $\langle 110 \rangle$  directions, 10 mm  $\times$  10 mm) was prepared by first annealing at 600 °C for 10 h in the UHV chamber, followed by a 5-nm-thick MgO seed layer growth at 500 °C. A 5-nm-thick Fe film was deposited on half of the substrate using

\*jjiali83@pku.edu.cn

†qiu@berkeley.edu

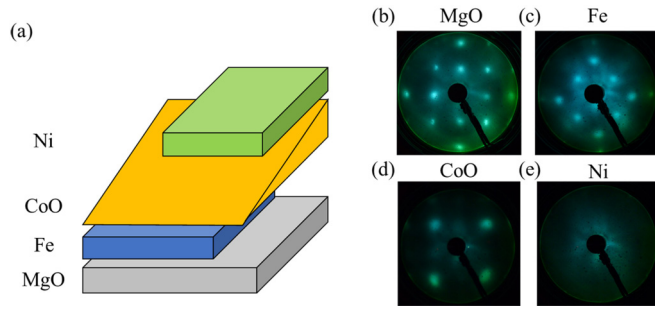


FIG. 1. (a) Schematic drawing of Ni/CoO bilayer and Ni/CoO/Fe trilayer samples. LEED patterns from (b) MgO(001) substrate after MgO seed layer growth at 130 eV, (c) 5-nm Fe layer at 184 eV, (d) 6.5-nm CoO layer at 129 eV, and (e) 2-nm Ni layer at 130 eV.

a knife-edge shutter. Then a wedged CoO film (0–7.5 nm) was grown by a reactive deposition of Co under an oxygen pressure of  $1.5 \times 10^{-6}$  Torr on the whole area of the MgO substrate by moving the substrate behind the shutter during the CoO growth. A 2-nm Ni film was grown on top of the whole substrate. Therefore we prepared Ni/CoO bilayers and Ni/CoO/Fe trilayers on the same substrate under the same condition (Fig. 1). Low-energy electron diffraction (LEED) at each stage of the growth shows the formation of single-crystalline bcc Fe and fcc CoO films with Fe[100]/CoO[110]/MgO[110] and polycrystalline Ni film [18,19].

Finally, the sample is capped by a 2-nm MgO layer as a protective layer and was brought to Beamline 6.3.1 at

the Advanced Light Source for magnetic measurement using XMCD and XMLD. Since XMCD measures the projection of the magnetization along the x-ray direction and that magnetic field can be applied only in the x-ray direction at Beamline 6.3.1, we probed the in-plane and out-of-plane component of the FM magnetization by taking the hysteresis loops at different incidence angle ( $\theta$ ) of the circular polarized x ray [12]. For an out-of-plane hysteresis loop, it is straightforward to take the hysteresis loop at normal incident of the x rays ( $\theta = 0^\circ$ ). For the in-plane component of the magnetization, grazing incidence of the x rays ( $\theta \neq 0^\circ$ ) was used for the measurement so that the in-plane component of the magnetic field switches the in-plane magnetization [Figs. 2(d) and 2(g)]. Since it is known that CoO on vicinal MgO(001) has its easy magnetization axis parallel to the steps and that the FM/CoO interfacial coupling favors a perpendicular alignment between the FM and CoO spins [18], all low-temperature (LT) states of the sample at Beamline 6.3.1 were achieved by cooling the sample with an in-plane magnetic field applied perpendicularly to the atomic steps of the vicinal surface (y axis in Fig. 2).

### III. RESULTS AND DISCUSSION

We first studied the magnetic properties of Ni(2 nm)/CoO(6.5 nm) bilayers grown on vicinal MgO(001) through element-specific XMCD and XMLD measurements. Figures 2(b) and 2(c) show the Ni hysteresis loops taken at normal incidence ( $\theta = 0^\circ$ ) [Fig. 2(a)] at temperatures of 350 and 78 K, respectively. The hard-axis loops with

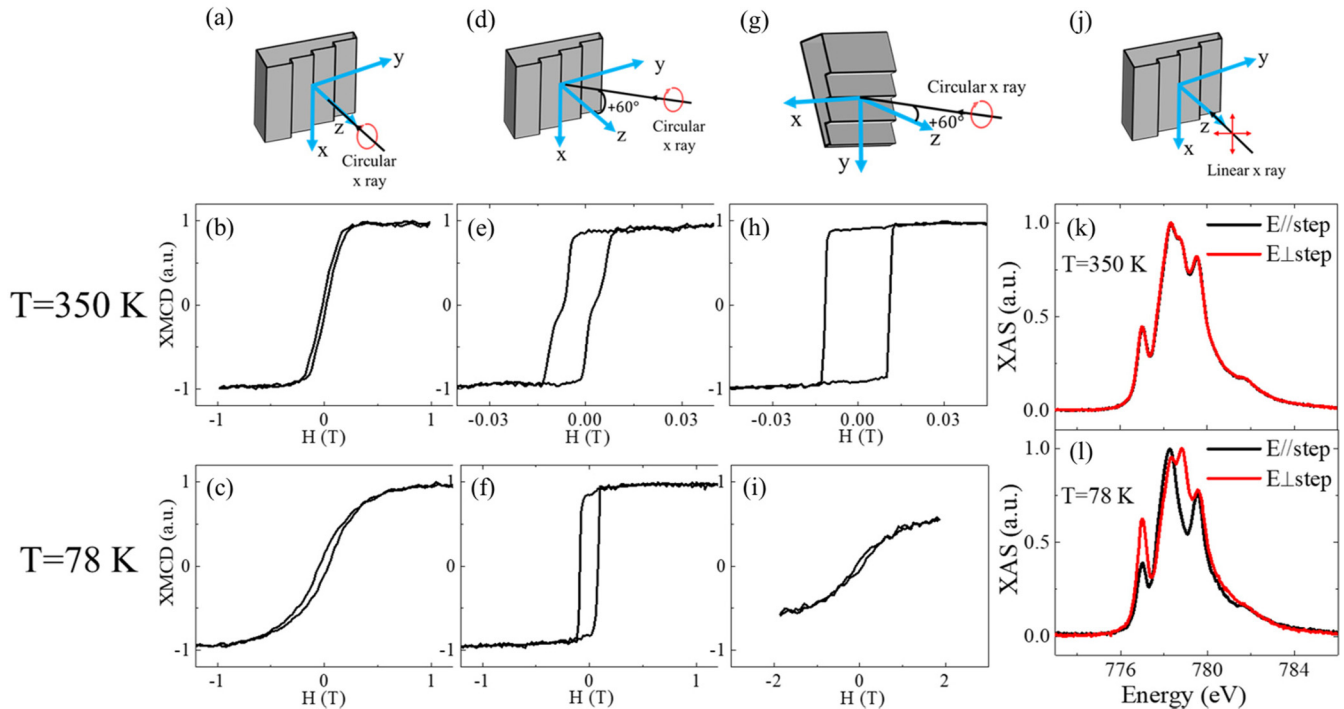


FIG. 2. Schematic drawing of different conditions for (a,d,g) Ni XMCD hysteresis loop measurement and (j) CoO XLD measurement from Ni(2 nm)/CoO(6.5 nm)/vicinal MgO(001) sample. The magnetic field is applied along the x-ray direction. (b,e,h) and (c,f,i) show the Ni hysteresis loops at 350 and 78 K, respectively. (k,l) show the Co  $L_3$  edge absorption spectra with linearly polarized x ray at normal incidence as shown in (j) at 350 and 78 K, respectively. The result shows that the CoO is AFM ordered at 78 K with its spins in plane and parallel to the atomic steps. As a consequence of the Ni/CoO  $90^\circ$  coupling, the fully in-plane Ni magnetization changes its EA direction from the parallel to the perpendicular direction of the atomic steps.

zero remanence at both high and low temperatures show that the easy axis (EA) of Ni magnetization is fully in the plane of the film at both high temperature (HT) and LT. The greater saturation field at LT could be attributed to the enhancement of the demagnetization field due to the increased Ni magnetization at LT. Since the Néel temperature of the 6.5-nm CoO is between 78 and 350 K [18,20], the result of Figs. 2(b) and 2(c) shows that the AFM order of the CoO film in the Ni/CoO bilayer does not change the Ni magnetization EA from in plane towards the out-of-plane directions. To determine the in-plane EA of the Ni magnetization, Ni hysteresis loops were taken at  $\theta = 60^\circ$  with the x-ray incident plane perpendicular and parallel to the atomic steps of the substrate [Figs. 2(d) and 2(g)], respectively. At 350 K, the Ni magnetization exhibits a double-split hard-axis (HA) character for the in-plane component of the magnetic field perpendicular to the steps [Fig. 2(e)] and an EA square-shape loop for the in-plane component of the magnetic field parallel to the steps [Fig. 2(h)], indicating that the step-induced magnetic anisotropy favors the Ni magnetization parallel to the atomic steps above the CoO Néel temperature in the Ni/CoO bilayer on vicinal MgO(001) [7,8,18]. At 78 K, however, the Ni magnetization exhibits the EA square shape for in-plane magnetic field perpendicular to the steps [Fig. 2(f)] and a HA loop for in-plane magnetic field parallel to the steps [Fig. 2(i)], showing that the Ni/CoO interfacial magnetic coupling [21] switches the Ni EA from a parallel to perpendicular direction relative to the steps. This EA switching and the much greater HA saturation field show a stronger Ni/CoO magnetic coupling than the step-induced anisotropy. This phenomenon has also been observed in other systems such as in Fe/CoO [17], Fe/NiO [22], and Fe/FeF<sub>2</sub> [23]. To explore the CoO spin structure and its coupling to the Ni in Ni/CoO system, CoO x-ray absorption spectra (XAS) were taken at the Co<sup>2+</sup> L<sub>3</sub> edge with the linear polarization of the x rays parallel and perpendicular to the steps at normal incidence [Fig. 2(j)]. The spectra difference [i.e., x-ray linear dichroism (XLD)] is zero at 350 K [Fig. 2(k)] but nonzero at 78 K [Fig. 2(l)], indicating the AFM origin of the Co<sup>2+</sup> L<sub>3</sub> edge XLD at 78 K [24,25]. The peak intensities at 777 and 778.8 eV are lower for  $E//\text{step}$  than for  $E\perp\text{step}$  ( $E$  is the polarization direction of the x rays), indicating that the CoO AFM spins are parallel to the steps along the (110) directions [14,18]. Therefore the coupling between Ni and CoO is confirmed to be a 90° coupling, which is consistent with the previously reported result [21]. To make a brief summary of the Ni/CoO/vicinal MgO(001) result, the Ni magnetization is in plane and parallel to the steps at 350 K (above the CoO Néel temperature), and is in plane and perpendicular to the steps at 78 K (below the CoO Néel temperature) with the CoO spins parallel to the steps.

Next we discuss the result of Ni/CoO/Fe/vicinal MgO(001). At 350 K, the Ni magnetization exhibits double-split HA loop with the in-plane magnetic field perpendicular to the steps [Fig. 3(e)] and EA loop with the in-plane magnetic field parallel to the steps [Fig. 3(h)], and a zero remanence HA loop for magnetic field in the out-of-plane direction [Fig. 3(b)]. The above result shows that the Ni magnetization in Ni/CoO/Fe trilayers behaves similarly to that in Ni/CoO bilayers; i.e., the Ni magnetization is fully in plane and parallel to the steps at 350 K. Below the CoO Néel temperature, we obtained

the Ni EA loop at  $\theta = 60^\circ$  with the in-plane magnetic field perpendicular to the atomic steps [Fig. 3(f)], and a HA loop with the in-plane magnetic field parallel to the atomic steps [Fig. 3(i)]. At the normal incidence of the x rays, the Ni magnetization exhibits a loop with a large remanence at 78 K [Fig. 3(c)] which is different from the situation for Ni/CoO bilayers. The above results indicate that the Ni magnetization in the Ni/CoO/Fe trilayer at 78 K has a canted remanence towards the out-of-plane orientation.

To make sure that the Ni spin canting is from the CoO AFM order rather than from other temperature effect (for example, temperature-dependent magnetocrystalline anisotropy), we measured the Ni hysteresis loops at 78 K as a function of the CoO thickness with the incident x rays in the  $yz$ -plane. Because the step-induced anisotropy is smaller than the coercivity [Fig. 3(e)], Ni spin canting in the  $yz$  plane can be easily reflected in the difference between hysteresis loops taken at  $+\theta$  and  $-\theta$ . For Ni/CoO (0.6 nm)/Fe, where the 0.6-nm CoO has a Néel temperature lower than 78 K, the Ni hysteresis loops have almost identical shapes for  $\theta = 30^\circ$  and  $\theta = -30^\circ$  [Fig. 4(a)], showing the absence of the Ni spin canting. For Ni/CoO (6.8 nm)/Fe, where the CoO is AFM ordered at 78 K, the Ni hysteresis loops are obviously different for  $\theta = 30^\circ$  and  $\theta = -30^\circ$  [Fig. 4(b)], showing a spin canting behavior of the Ni layer due to the CoO AFM order. In addition, the much greater remanence at  $\theta = 30^\circ$  than at  $\theta = -30^\circ$  shows that the Ni spin canting is towards the  $+\theta$  direction. The difference between the Ni magnetic remanences at  $\theta = 30^\circ$  and  $\theta = -30^\circ$  actually develops drastically above 1.2-nm CoO thickness [Fig. 4(c)]. Noting that the Néel temperature of the CoO film increases with CoO film thickness [18,20] and that the CoO critical thickness from paramagnetic to antiferromagnetic state is  $\sim 1\text{--}3$  nm at low temperature [18], the result of Fig. 4(c) further proves that the Ni spin canting at 78 K must come from the CoO AFM order. To quantitatively determine the EA direction of the Ni magnetization, hysteresis loops were measured at different x-ray incident angles  $\theta$  to obtain the relative magnetic remanence ( $M_r/M_S$ ) as a function of  $\theta$  [Figs. 4(d) and 4(e)]. Since the magnetic remanence taken for x ray in the  $yz$  plane represents the projection of the Ni EA along the x-ray incident direction in the  $yz$  plane, we use the following formula to fit the  $\theta$ -dependent remanence signal:

$$M_r/M_S = |\cos(\theta - \theta_{\text{Ni}})|. \quad (1)$$

Here  $\theta_{\text{Ni}}$  is defined as the angle between the Ni EA direction and the sample normal direction. We obtained  $\theta_{\text{Ni}} = 90^\circ$  at 350 K (i.e., the Ni EA is in plane at high temperature), and  $\theta_{\text{Ni}} = 57^\circ$  at 78 K (i.e., the Ni EA cants  $33^\circ$  away from the sample surface in the  $yz$  plane). This value is apparently larger than the vicinal angle ( $7^\circ$ ) of the MgO(001) substrate. In contrast to the spin canting of Ni layer, the Fe magnetization in the Ni/CoO/Fe trilayer remains in plane at 78 K. This point was proved by incidence angle ( $\theta$ )-dependent remanence signal [Fig. 4(d)], where the remanence signal shows a symmetric behavior around  $0^\circ$ . To prove that vicinal surface is crucial in producing the spin canting, we also performed measurements on the Ni/CoO/Fe trilayer grown on flat MgO(001). The result [Fig. 4(e)] shows an absence of the Ni spin canting in this case, proving the necessary condition of the vicinal surface for the Ni spin canting. The small nonzero Ni remanence

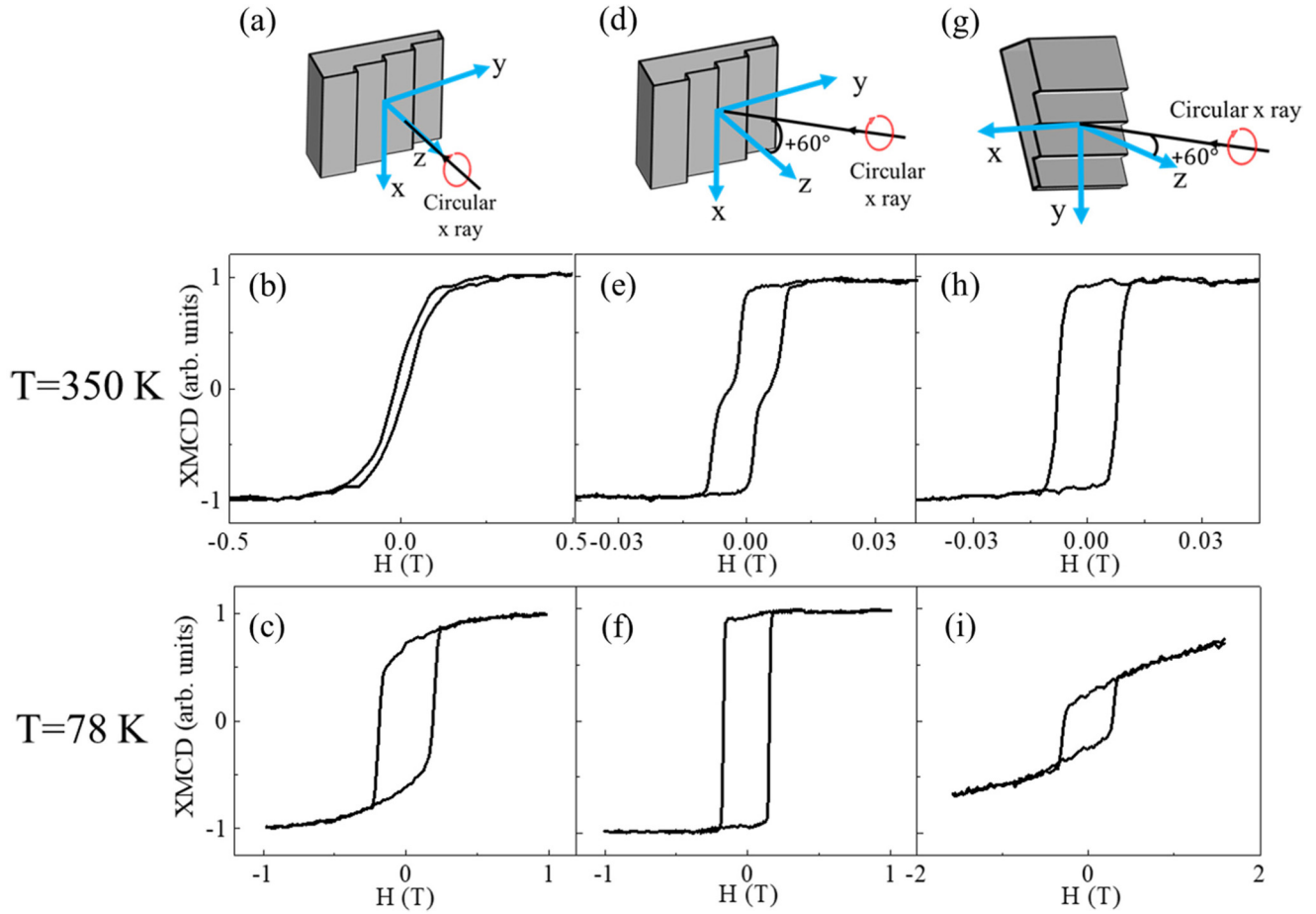


FIG. 3. Ni hysteresis loops from Ni(2 nm)/CoO(6.5 nm)/Fe(5 nm)/vicinal MgO(001) taken under different conditions shown in (a–c) for the corresponding column. The magnetic field is applied along the x-ray direction. The result shows that while the Ni magnetization at 350 K is in plane and is parallel to the steps, the Ni magnetization at 78 K is canted towards the out-of-plane direction in the  $yz$  plane.

for field along the hard axis could either come from small misalignment of the magnetic field to the sample holder, or from higher-order magnetic anisotropy in Ni film. The exchange coupling in the FM/FM system has been reported to induce fourfold magnetic anisotropy in addition to the dominant uniaxial magnetic anisotropy [15,26], which could introduce the nonzero remanence for field along the HA of uniaxial anisotropy. However, since the high-remnance parts of Ni can be well fitted by Eq. (1), we will only consider the uniaxial anisotropy later.

The in-plane Ni EA magnetizations in the Ni/CoO system and the canted Ni EA magnetization in Ni/CoO/Fe systems on vicinal MgO(001) at 78 K show that the CoO spins must be different in the bilayer and trilayer systems; i.e., the addition of the CoO/Fe magnetic coupling has made the CoO spin configuration in the Ni/CoO/Fe trilayers different from that in the Ni/CoO bilayers. To determine the CoO compensated bulk spin orientation in experiment, we measured x-ray absorption spectra at the  $\text{Co}^{2+} L_3$  edge at different x-ray incident angles with the linear polarization in the incident plane [27,28]. Figures 5(a) and 5(d) show the spectra at 78 K at normal and grazing incidence of the x rays with the incident plane perpendicular and parallel to the atomic steps, respectively. There is an obvious difference at the peaks of  $\sim 777, 778.8,$

and 779.6 eV. Van der Laan *et al.* pointed out that one has to be careful in analyzing the spectra because it is very easy to make a mistake in the AFM spin-axis determination due to the lattice distortion effect in the XLD spectrum [29]. In particular, the CoO  $L_3$  edge at  $\sim 777$  eV could be attributed to a charge anisotropy rather than a magnetic anisotropy. To avoid this complexity factor, we define the CoO  $R_{L_3}$  ratio as the intensity ratio of the peak at  $\sim 778.3$  eV over the peak at  $\sim 778.8$  eV as denoted by the two arrows in Fig. 5(d).

Figures 5(b) and 5(e), and 5(c) and 5(f) show the CoO  $R_{L_3}$  ratio as a function of the x-ray incidence angle  $\theta$  from Ni/CoO bilayers and Ni/CoO/Fe trilayers on vicinal MgO(001), respectively. All these  $R_{L_3}(\theta)$  curves show a clear quadratic dependence on the sinusoidal  $\theta$ , and indeed can be well fitted by  $R_{L_3}(\theta) = A \cos(\theta - \theta_0)^2 + B$  [24,30,31]. Comparing the CoO  $R_{L_3}(\theta)$  curves at 78 and 350 K, the Ni/CoO bilayers display almost identical amplitudes of  $R_{L_3}(\theta)$  curves for x-ray incident plane perpendicular to the steps [Fig. 5(b)], and an obvious difference for the x-ray incident plane parallel to the steps [Fig. 5(e)]. The XLDs at the Co  $L_3$  edge are contributed from both the crystal-field effect and the AFM order. While the AFM contribution vanishes above the Néel temperature, the crystal-field effect persists at high temperature [24,25]. Then the fact that the two curves in

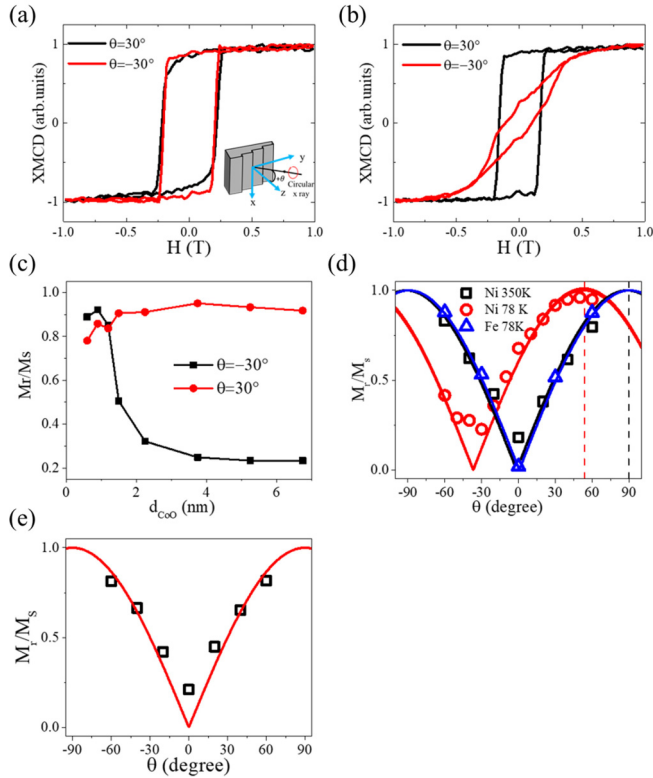


FIG. 4. Ni hysteresis loops from the Ni (2 nm)/CoO wedge (0–7.5 nm)/Fe (5 nm)/vicinal MgO(001) obtained at 78 K in the geometry of Fig. 2(a) at the x-ray incident angle of  $\theta = 30^\circ$  and  $\theta = -30^\circ$  with (a) 0.6-nm CoO and (b) 6.8-nm CoO. (c) Ni remanence as a function of CoO thickness at  $\theta = 30^\circ$  and  $\theta = -30^\circ$ . (d) Ni and Fe magnetic remanence as a function of  $\theta$  at 78 and 350 K from Ni (2 nm)/CoO (6.5 nm)/Fe (5 nm)/vicinal MgO(001). The solid lines are the fitting result using Eq. (1). The Ni EA direction is shifted from  $\theta_{\text{Ni}} = 90^\circ$  at 350 K to  $\theta_{\text{Ni}} = 57^\circ$  at 78 K. (e) Ni magnetic remanence as a function of  $\theta$  at 78 K from Ni(3 nm)/CoO(6 nm)/Fe(5 nm)/flat MgO(001). The minimum  $M_r/M_s$  at  $\theta = 0^\circ$  shows the absence of Ni spin canting in Ni/CoO/Fe grown on flat MgO(001).

Fig. 5(b) have amplitudes almost identical to the 350 K curve in Fig. 5(e) shows that these three curves are from the crystal-field effect. In order to single out the magnetic contribution in  $R_{L3}$ , we fit each  $R_{L3}$  using  $R_{L3}(\theta) = A \cos(\theta - \theta_0)^2 + B$  and use the difference of the fitted  $R_{L3}$  between 78 and 350 K,  $\Delta R_{L3} \equiv R_{L3}(78 \text{ K}) - R_{L3}(350 \text{ K})$  [Figs. 5(h) and 5(i)], as the magnetic contribution to the CoO XLD. For Ni/CoO biayers,  $\Delta R_{L3}$  reaches maximum at the normal incidence ( $\theta = 0^\circ$ ) for the x-ray incident plane parallel to the steps and is virtually constant for x-ray incident plane perpendicular to the steps [Fig. 5(h)], showing that the CoO spins in Ni/CoO/vicinal MgO(001) are in the film plane and parallel to the atomic steps. This result is the same as in the Fe/CoO/vicinal MgO(001) system [18]. The in-plane CoO spin orientation can be attributed to the compressive strain on the MgO(001) substrate ( $a_{\text{CoO}} = 4.26 \text{ \AA} > a_{\text{MgO}} = 4.21 \text{ \AA}$ ) [27,28].

Next we discuss the CoO XLD result in Ni/CoO/Fe/vicinal MgO(001). Figure 5(f) depicts the  $R_{L3}(\theta)$  curves at 78 and 350 K for the x-ray incident plane parallel to the steps. It is interesting to note that while the  $R_{L3}(\theta)$  at 350 K is similar to

that in the Ni/CoO bilayer, the  $R_{L3}(\theta)$  at 78 K has a smaller amplitude than that of the Ni/CoO bilayer system, indicating a reduction of the CoO spins parallel to the atomic steps (or equivalently a development of spin component in the  $yz$  plane) in the Ni/CoO/Fe compared to the Ni/CoO. Figure 5(c) depicts the  $R_{L3}(\theta)$  curves from Ni/CoO/Fe for the x-ray incident plane perpendicular to the steps. Note that while the  $R_{L3}(\theta)$  curve at 350 K is symmetric with respect to the surface normal direction and similar to that of the Ni/CoO bilayer, the  $R_{L3}(\theta)$  curve at 78 K in Ni/CoO/Fe exhibits an asymmetric behavior with its maximum appearing at an off-normal direction of the sample surface, showing that there exists a certain number of CoO spins in the  $yz$  plane in the Ni/CoO/Fe system which is consistent with the reduced CoO spins parallel to the steps. Quantitatively, Fig. 5(i) shows the  $\theta$  dependence of the  $\Delta R_{L3}$  for x-ray polarization parallel and perpendicular to the atomic steps. The evidently much larger  $\Delta R_{L3}$  for x-ray polarization parallel to the atomic steps shows that the dominant component of the CoO AFM spins is parallel to the steps, similar to that in the Ni/CoO bilayer system. However, the nonzero  $\Delta R_{L3}$  for x-ray polarization perpendicular to the steps, especially the occurrence of maximum XMLD at  $41^\circ$ , shows that the CoO AFM spins also have a canted component towards the out-of-plane direction in the  $yz$  plane [Fig. 5(g)]. This additional CoO component in the  $yz$  plane in the Ni/CoO/Fe trilayers is absent in the Ni/CoO bilayers and should be related to the Ni spin canting in the  $yz$  plane in the Ni/CoO/Fe trilayers. We will discuss this relation later in this paper.

The above result shows clearly that the Fe in Ni/CoO/Fe/vicinal MgO(001) causes a Ni spin canting in the  $yz$  plane as well as a CoO spin canting component in the  $yz$  plane. Note that if the Ni spin canting towards  $+\theta$  rather than  $-\theta$  in the  $yz$  plane breaks the inversion symmetry ( $y \rightarrow -y$ ), then it is natural to ask if this symmetry breaking is a result of the Ni/Fe interlayer coupling or a result of the Ni/CoO interfacial coupling due to the CoO  $yz$  component. The difference between these two mechanisms can be distinguished by an examination of whether the Ni magnetization direction is directly correlated to the Fe magnetization direction, i.e., if the Ni magnetization would be reversed after the reversal of the Fe magnetization. From the hysteresis loop measurement, the Ni layer from Ni/CoO/Fe/vicinal MgO(001) actually shows identical spin canting for both zero field cooling and field cooling, suggesting that the Ni spin canting is not from a direct coupling between the Fe and the in-plane Ni magnetizations. To prove this speculation, we did photoemission electron microscopy (PEEM) measurements after zero field cooling so that the in-plane Ni and Fe magnetizations would not be aligned to the same direction by a field cooling process. We imaged the ferromagnetic Ni and Fe domains by taking the ratio of left and right circularly polarized incident x rays at the corresponding Ni and Fe  $L_3$  absorption edges at 110 K after zero field cooling utilizing the element-resolved XMCD and XMLD effect. In our measurement, the x ray is at an incident angle of  $60^\circ$  with respect to the surface normal direction [Fig. 6(a)]. The sample was azimuthally rotated by about  $10^\circ$  to distinguish any possible FM magnetizations parallel to the atomic steps. Figures 6(b) and 6(e) show that there exist only Ni and Fe domains with their magnetization perpendicular to the steps (both the white and dark domains have magnetizations

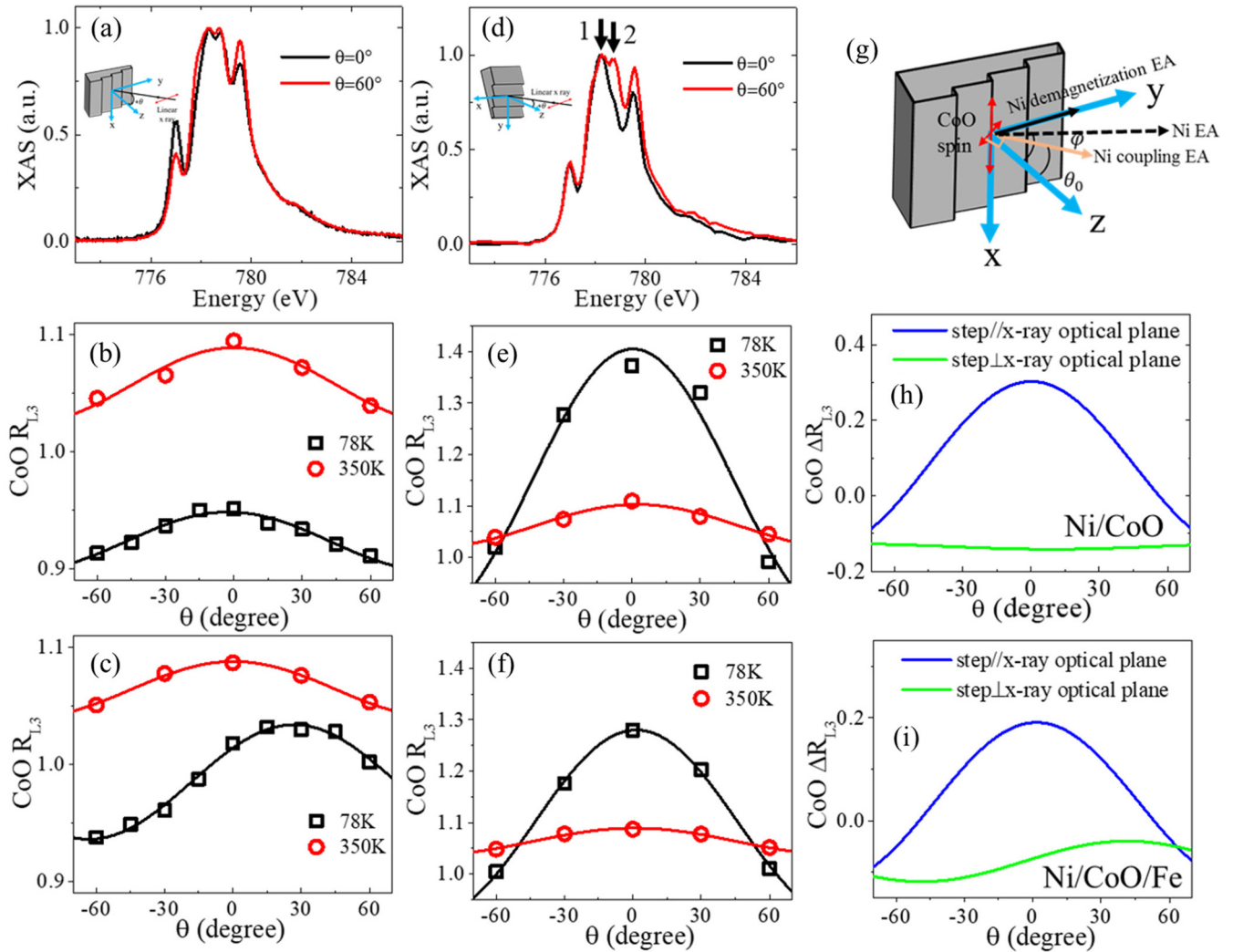


FIG. 5. (a,d) Co  $L_3$  edge spectra from Ni(2 nm)/CoO(6.5 nm)/Fe(5 nm) with the incident x rays at normal ( $\theta = 0^\circ$ ) and grazing incidence ( $\theta = 60^\circ$ ). The x-ray linear polarization is in the incident plane. (b,e,h) and (c,f,i) show the CoO  $R_{L_3}$  ratio as a function of different grazing incidence angle  $\theta$  at both 78 and 350 K from Ni(2 nm)/CoO(6.5 nm) bilayers and Ni(2 nm)/CoO(6.5 nm)/Fe(5 nm) trilayers, respectively. The x-ray incident plane is (a–c) perpendicular to the steps, and (d–f) parallel to the steps. (h,i)  $\Delta R_{L_3} \equiv R_{L_3}(78\text{ K}) - R_{L_3}(350\text{ K})$  is the magnetic contribution to the  $R_{L_3}$ . (g) Schematic drawing of the Ni EA and CoO spin orientation.

perpendicular to the steps but with opposite magnetization directions). Although it is difficult to identify the Ni spin canting configuration from the PEEM image due to the fixed grazing angle of the incident x rays, the Ni magnetization should be pointing to an angle of  $\theta_{\text{Ni}} = 57^\circ$  towards the out-of-plane direction as determined by the hysteresis loop measurement. The most important PEEM result is that the Ni and Fe magnetizations exhibit different domain patterns [Figs. 6(b) and 6(e)] although both are perpendicular to the steps, showing a lack of direct correlation between the Ni and Fe magnetizations across the 6.5-nm CoO layer. This result shows that the Ni and Fe spin orientations should be determined separately by their couplings to the CoO at the corresponding interfaces rather than by a direct interlayer coupling; i.e., the effect of the Fe is to introduce a uniaxial anisotropy rather than a unidirectional anisotropy to the Ni layer to cause its spin canting towards the  $+\theta$  direction. In principle, a vicinal surface is inherently asymmetric under

the inversion of  $y \rightarrow -y$ , thus permitting inversion symmetry breaking between  $+\theta$  and  $-\theta$ . The CoO AFM domains in the Ni/CoO/Fe trilayer were also imaged using the XMLD effect. Figure 6(d) showed that the CoO AFM domain is a single domain with the major component of the CoO spins parallel to the steps. These PEEM images clearly demonstrate the  $90^\circ$  coupling at both Ni/CoO and CoO/Fe interfaces, which is the same as that in Ni/CoO and CoO/Fe bilayer systems [14]. Again the CoO canting component in the  $yz$  plane cannot be picked up by PEEM due to the measurement constraint. We then imaged the uncompensated spin of the CoO layer using the XMCD effect. The result [Fig. 6(c)] shows the existence of uncompensated FM Co which has the same domain pattern as that of the Ni layer, indicating that the uncompensated FM Co spins are located at the Ni/CoO interface. The existence of uncompensated AFM spins at the top interface of the FM/AFM/FM trilayer system was also reported in other systems [32]. The same domain pattern of the

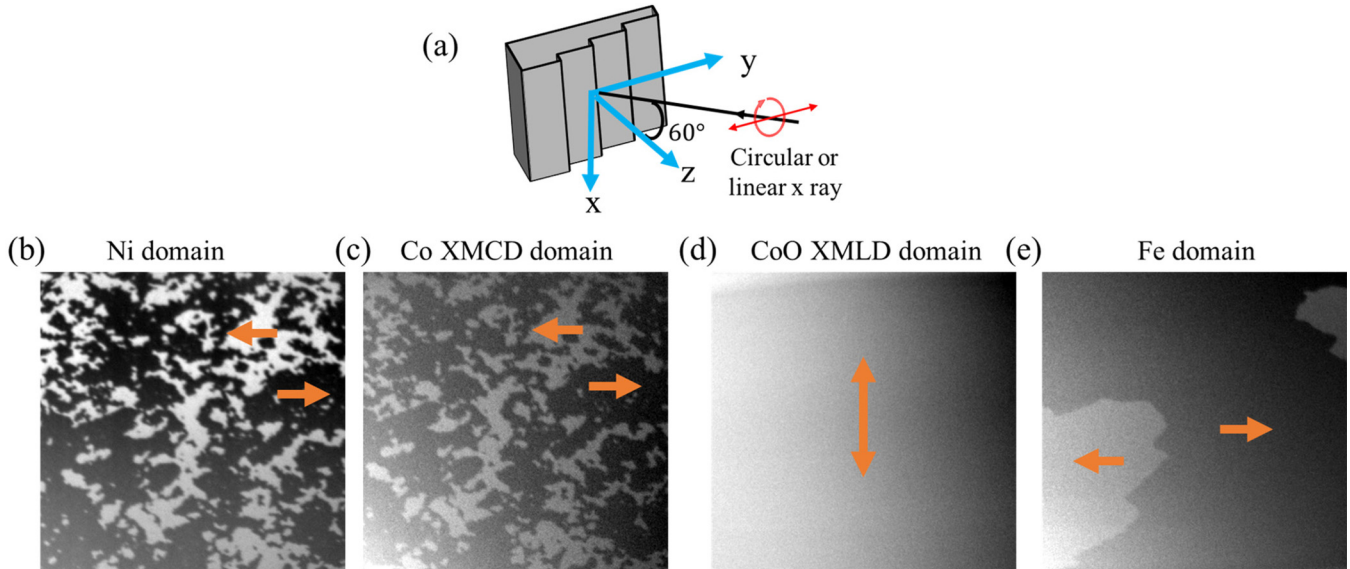


FIG. 6. (a) PEEM measurement condition. (b) Ni and (e) Fe XMCD images and (c) Co XMCD and (d) XMLD images taken from Ni (2 nm)/CoO (6.5 nm)/Fe (5 nm). The scale of the views is  $22 \times 22 \mu\text{m}$ .

uncompensated CoO spins as the Ni domain pattern suggests that the ferromagnetic Co spins at the Ni/CoO interface behave more likely as part of the FM Ni rather than being responsible for the spin canting of the Ni layer.

To explore the origin of spin canting in the CoO layer, we also studied the CoO/Fe bilayer on vicinal MgO(001). For this CoO/Fe bilayer without Ni, the Fe magnetization exhibits an easy-axis loop at  $60^\circ$  incidence of the x rays and a hard-axis loop at normal incidence of the x rays [Fig. 7(a)]. The remanence as a function of the x-ray incidence angle shows a symmetric behavior around  $0^\circ$ , proving an in-plane orientation of

the Fe spin magnetization [Fig. 7(b)], which is the same as the Fe in the Ni/CoO/Fe trilayer shown in Fig. 4(d). Figures 7(c) and 7(d) depict the  $\theta$  dependence of the  $\Delta R_{L3}$  of the CoO layer from the CoO/Fe bilayer for x-ray polarization perpendicular and parallel to the atomic steps. The much larger amplitude of the  $R_{L3}(\theta)$  curve at 78 K for x-ray polarization parallel to the atomic steps indicates that the dominant CoO AFM spins are parallel to the steps [Fig. 7(d)]. The nonzero  $\Delta R_{L3}$  for x-ray polarization perpendicular to steps with the maximum position of  $R_{L3}(\theta)$  at  $\theta \sim 15^\circ$  indicates the existence of a canted CoO AFM spin component in the  $yz$  plane [Fig. 7(c)]. The spin canting of the CoO layer is retained in the CoO/Fe bilayer without a Ni layer, confirming the fact that the canting of CoO AFM spins originate from CoO/Fe interfacial coupling. Note the CoO spin canting angle in the Co/Fe bilayer is different from that in the Ni/CoO/Fe trilayer, which might be attributed to the influence of the magnetic interaction between Ni and CoO [33], or different interfacial anisotropies between the MgO/CoO interface and the Ni/CoO interface, respectively [34].

It is well known that growing CoO on top of Fe results in the formation of a Fe oxidation layer (FeCo alloy or FeCoO ferrite layer) at the CoO/Fe interface which could influence the magnetic properties of the CoO/Fe system [35–37]. There have been contradicting results on the effect of this ferrite layer, where some works reported an important effect in mediating the exchange coupling [38,39] while other works reported no observable effect [40]. Different from the high-temperature growth of the AFM layer, all the films in our work were deposited at room temperature which should greatly suppress the intermixing and formation of the ferrite layer. Then it is natural to ask what the role is of the Fe oxidation layer in the CoO spin canting. To single out the interfacial Fe oxide feature from the overall Fe spectrum, we prepared a sample of CoO/Fe/vicinal MgO(001) in which the Fe was grown into a wedge shape. The XAS at the Fe  $L_3$  edge clearly shows a split double peak at 707.3 and 708.5 eV, respectively [Fig. 8(a)]. Similar to what has been reported in the literature, the

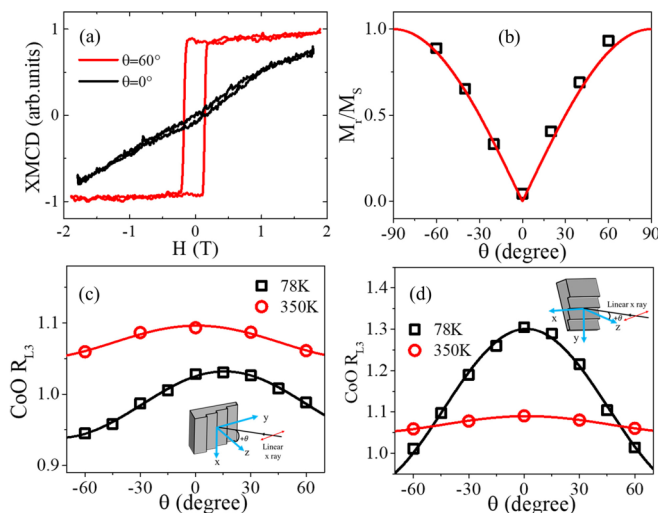


FIG. 7. (a) Fev XMCD hysteresis loop with x-ray at normal incidence ( $\theta = 0^\circ$ ) and grazing incidence ( $\theta = 60^\circ$ ) from CoO(6.5 nm)/Fe(5 nm)/vicinal MgO(001). (b) shows the remanence signal of the Fe layer at different incidence angle  $\theta$ . CoO  $R_{L3}$  ratio as a function of different grazing incidence angle  $\theta$  at both 78 and 350 K with x-ray incident plane (c) perpendicular to steps and (d) parallel to steps. The insets of (c,d) show the measurement geometries.



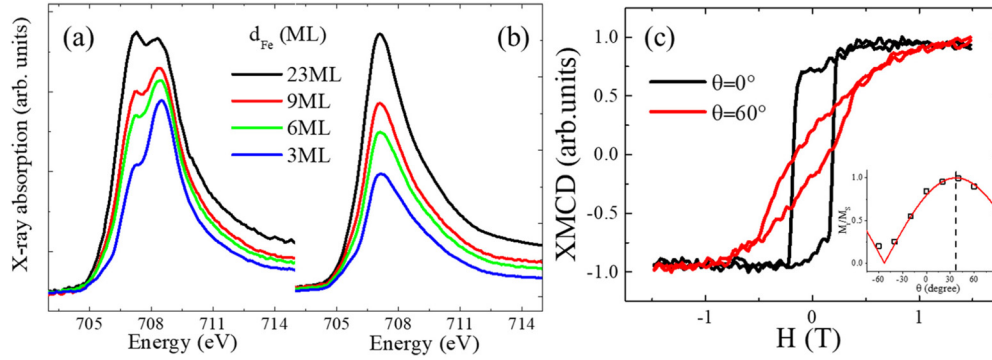


FIG. 8. XAS at the Fe  $L_3$  edge from (a) CoO(1.2 nm)/Fe wedge/vicinal MgO(001) and (b) CoO(1.2 nm)/Co(0.7 nm)/Fe wedge/vicinal MgO(001). (c) Ni XMCD hysteresis loop with x ray at normal incidence ( $\theta = 0^\circ$ ) and grazing incidence ( $\theta = 60^\circ$ ) from Ni(2 nm)/CoO(3 nm)/Co(0.7 nm)/Fe(5 nm)/vicinal MgO(001). The Ni remanence as a function of the x-ray incidence angle (inset) shows the same Ni spin canting behavior after adding the Co buffer layer.

double peak's intensity relative to the whole Fe peak intensity increases with decreasing the Fe film thickness, showing that the oxidized Fe is localized at the CoO/Fe interface [41]. Then the key question is whether the interfacial Fe oxide or FeCoO layer just serves to mediate a magnetic coupling between the FM Fe and the AFM CoO or are any specific chemical states of the Fe oxide or FeCoO interfacial layer critical to the Ni spin canting. To answer this question, we grew another sample in which a Co buffer layer (0.7 nm) was grown on top of the Fe layer before leaking oxygen into the chamber for the growth of the single-crystalline CoO film [35,36]. The LEED result confirms the single-crystalline growth of the Co buffer layer. The Fe XAS [Fig. 8(b)] exhibits only a single peak at 707.3 eV, indicating the absence of any Fe oxide layer; i.e., the interfacial oxide layer should be formed at the CoO/Co interface in this sample. Then we measured Ni magnetic properties in this new sample of Ni/CoO/Co/Fe/vicinal MgO(001) to study the spin canting in the Ni layer [Fig. 8(c)]. The Ni spin clearly exhibits a spin canting behavior similar to that in the Ni/CoO/Fe system without the Co buffer layer, i.e., a larger remanence at normal incidence of the x rays than at grazing incidence of the x rays with the minimum of remanence occurring at an off normal direction of the sample surface. This result proves that different oxide chemical states between the AFM CoO and the FM Fe may only modulate the CoO-Fe coupling strength and the Ni canting angle value but will not change the Ni spin canting behavior.

To quantitatively analyze the Ni spin canting in the Ni/CoO/Fe trilayer, we consider the competition between the Ni/CoO interfacial coupling energy and demagnetization energy of the Ni layer in the remanence state. For the configuration shown in Fig. 5(g), i.e., for Ni magnetization in the  $yz$  plane, the Ni magnetization is perpendicular to the steps so that its coupling to the CoO spin component parallel to the steps remains a constant but its coupling to the CoO spin component in the  $yz$  plane varies with its spin canting angle  $\varphi$ . Then the Ni energy density is given by

$$E = 2\pi M^2 \cos^2 \varphi - K \cos^2(\varphi - \theta_0). \quad (2)$$

Here  $M$  is the Ni saturation magnetization,  $K$  is the uniaxial anisotropy constant induced by the magnetic coupling between Ni and the  $yz$  component of the CoO spins in the  $yz$  plane, and

$\theta_0$  is the EA angle due to this Ni/CoO coupling in the  $yz$  plane which can be obtained from the  $R_{L3}(\theta)$  curve in Fig. 5(i). The final direction of the Ni EA ( $\varphi_0$ ) can be obtained by minimizing the energy density with respect to the Ni magnetization angle  $\frac{\partial E}{\partial \varphi} = 0$ :

$$\tan 2\varphi_0 = \frac{K/2\pi M^2 \sin 2\theta_0}{K/2\pi M^2 \cos 2\theta_0 - 1}. \quad (3)$$

The value of  $\theta_0$  is determined to be  $41^\circ$  from the fitting result in Fig. 5(i). Then for the value of  $\varphi_0 = 57^\circ$  determined from Fig. 4(d), an anisotropy constant of  $K/2\pi M^2 = 1.7$  is needed to generate the Ni spin canting. Then the question is if this value is reasonable or not. Although we cannot determine  $K$  directly in experiment, we could have a rough estimation of its value. With the following four facts—(1) the coupling of the Ni spin to the  $yz$  component of the CoO spin ( $S_{\text{CoO},yz}$ ) generates the Ni uniaxial anisotropy in the  $yz$  plane ( $K$ ); (2) the coupling of the Ni spin to the  $xy$  component of the CoO spin ( $S_{\text{CoO},xy}$ ) generates the Ni uniaxial anisotropy in the  $xy$  plane ( $K'$ ) which is proportional to the saturation field in Fig. 3(i) ( $H_{S,xy} = 2K'/M \sim 3.5\text{--}4\text{ T} \times \sin 60^\circ = 3.0\text{--}3.5\text{ T}$ ); (3)  $(K/K')^2 \sim (S_{\text{CoO},yz}/S_{\text{CoO},xy})^2$  is the ratio of the two XMLD amplitudes in Fig. 5(i), i.e.,  $(K/K')^2 \sim 0.079/0.310 = 0.255$  or  $K/K' \sim 0.5$ ; and (4) the out-of-plane saturation field of Ni is  $H_{S,z} = 4\pi M \sim 0.7\text{ T}$  [Fig. 2(c)]—we estimate the anisotropy  $K$  to be  $K/2\pi M^2 = (K/K')(2K'/M)/(4\pi M) = (K/K')(H_{S,xy}/H_{S,z}) \sim 0.5 \times (3.0\text{--}3.5)/0.7 \sim 2.1\text{--}2.5$  which is more but roughly agrees with the value of 1.7 needed for the  $57^\circ$  Ni spin canting. The next question is why we did not observe obvious spin canting for Fe magnetization which should also be coupled to the  $yz$  component of the CoO spins. Note that the Fe magnetization is about 4 times the Ni magnetization; the  $K/2\pi M^2$  value for 5-nm Fe should be scaled down by a factor of  $(1/4^2)(2\text{ nm}/5\text{ nm}) \sim 0.025$  which gives  $K/2\pi M^2 \sim 1.7 \times 0.025 = 0.043$  for 5-nm Fe. Then according to Eq. (2), the Fe magnetization should have an EA at  $\varphi_0 \sim 88.7^\circ$  or be canted only  $\sim 1.3^\circ$  towards the out-of-plane direction, which explains why we did not observe the Fe spin canting.

From all the above results, it is clear that the most important finding of this work is that the CoO AFM spins in Ni/CoO/Fe/vicinal MgO(001) system are canted towards the

out-of-plane direction at a sizable angle, which consequently causes the Ni spin canting due to the Ni/CoO interfacial magnetic coupling. The absence of the CoO spin canting in Ni/CoO/vicinal MgO(001) demonstrates the crucial role of Fe in the CoO spin canting. The insertion of the Co layer at the CoO/Fe interface eliminates the oxidization of the Fe layer, but keeps the spin canting, indicating the independence of the Fe oxidization state. All the films in our sample are deposited at normal incidence from a commercial four-pocket evaporator, thus ruling out any uniaxial anisotropy induced by oblique incidence deposition [42]. Then is it the lattice distortion effect or the CoO/Fe interfacial magnetic coupling effect? For the lattice distortion effect, a compression in the film plane usually promotes the CoO or NiO towards in-plane spin alignment. For example, a smaller lattice constant of Ag than of MgO makes NiO/Ag(001) in-plane spin orientation as opposed to the out-of-plane NiO/MgO(001) orientation, and a greater CoO lattice constant than NiO has an in-plane spin orientation in CoO/MgO(001) [18,30]. Then the smaller lattice constant of Fe compared to that of MgO should promote more in-plane spin orientation of CoO on Fe/MgO(001) than of MgO(001). This point is further confirmed by our measurement on Ni/CoO/Fe/flat MgO(001) which shows in-plane CoO AFM spins. Therefore the CoO/Fe magnetic coupling is necessary to induce the CoO spin canting in Ni/CoO/Fe/vicinal MgO(001). Furthermore, the Ni spin canting towards  $+\theta$  as opposed to  $-\theta$  and the fact that the spin canting is absent in Ni/CoO/Fe/flat MgO(001) [Fig. 4(e)] show that the vicinal surface is necessary in producing the CoO spin canting. Therefore we conclude that it is the CoO/Fe interfacial magnetic coupling on the vicinal surface that causes the CoO spin canting. The result that Ni in Ni/CoO/Fe/vicinal MgO(001) has a step-induced anisotropy at high temperature [Fig. 3(e)] shows the persistence of vicinal steps on the top CoO surface. In the Néel-pair-bonding model used to understand the step-induced anisotropy, the magnetic anisotropy is determined by the spin-orbit interaction through the nearest-neighbor electronic hybridization [7,8]. The necessary condition of the CoO/Fe magnetic coupling in producing the CoO spin canting shows that any explanations involving the Néel-pair-bonding model have to include the ferromagnetic state of Fe. We noticed one recent paper report that the change of interfacial bond angles induced dramatic perpendicular

magnetic anisotropy in  $(\text{La}_{1-x}\text{Sr}_x\text{MnO}_3/\text{SrIrO}_3)$  superlattices [43]. Our result also indicates the missing chemical bonds at the step-edge atoms lead to the perpendicular anisotropy in CoO film. With all experimental results presented in this paper, the last unanswered question is how the vicinal surface of a ferromagnetic Fe induces the CoO spin canting. We could not answer this question and would like to keep it open for the community and future works to address.

#### IV. SUMMARY

Utilizing XMCD, XMLD, and PEEM measurements, we find that the CoO spins in Ni/CoO/vicinal MgO(001) are in the film plane and parallel to the atomic steps, but consist of the additional spin component that is canted towards the out-of-plane direction in Ni/CoO/Fe/vicinal MgO(001). Consequently, the Ni magnetization in Ni/CoO/vicinal MgO(001) is in the film plane and perpendicular to the atomic steps, but cants towards the out-of-plane direction in Ni/CoO/Fe/vicinal MgO(001). This result reveals that the CoO/Fe magnetic interfacial coupling on the vicinal surface could modify the CoO spin configuration and consequently induces a uniaxial magnetic anisotropy in the Ni film that favors a spin canting orientation.

#### ACKNOWLEDGMENTS

This work is supported by the US Department of Energy, Office of Science, Office of Basic Energy Sciences, Materials Sciences and Engineering Division under Contract No. DE-AC02-05CH11231 (van der Waals heterostructures program, KCWF16), National Science Foundation Grant No. DMR-1504568, Future Materials Discovery Program through the National Research Foundation of Korea (Grant No. 2015M3D1A1070467), Science Research Center Program through the National Research Foundation of Korea (Grant No. 2015R1A5A1009962), and National Key Research and Development Program of China (Grant No. 2016YFA0300804). The operations of the Advanced Light Source at Lawrence Berkeley National Laboratory are supported by the Director, Office of Science, Office of Basic Energy Sciences, and US Department of Energy under Contract No. DE-AC02-05CH11231.

- 
- [1] D.-s. Wang, R. Wu, and A. J. Freeman, *Phys. Rev. Lett.* **70**, 869 (1993).
  - [2] Z. Q. Qiu, J. Pearson, and S. D. Bader, *Phys. Rev. Lett.* **70**, 1006 (1993).
  - [3] J. Thomassen, F. May, B. Feldmann, M. Wuttig, and H. Ibach, *Phys. Rev. Lett.* **69**, 3831 (1992).
  - [4] B. N. Engel, C. D. England, R. A. Van Leeuwen, M. H. Wiedmann, and C. M. Falco, *Phys. Rev. Lett.* **67**, 1910 (1991).
  - [5] S. Hashimoto, Y. Ochiai, and K. Aso, *J. Appl. Phys.* **67**, 2136 (1990).
  - [6] B. Schulz and K. Baberschke, *Phys. Rev. B* **50**, 13467 (1994).
  - [7] R. K. Kawakami, E. J. Escorcia-Aparicio, and Z. Q. Qiu, *Phys. Rev. Lett.* **77**, 2570 (1996).
  - [8] R. K. Kawakami, M. O. Bowen, Hyuk J. Choi, E. J. Escorcia-Aparicio, and Z. Q. Qiu, *Phys. Rev. B* **58**, R5924 (1998).
  - [9] J. Nogués and I. K. Schuller, *J. Magn. Magn. Mater.* **192**, 203 (1999).
  - [10] M. Kiwi, *J. Magn. Magn. Mater.* **234**, 584 (2001).
  - [11] M. Grimsditch, A. Hoffmann, P. Vavassori, H. T. Shi, and D. Lederman, *Phys. Rev. Lett.* **90**, 257201 (2003).
  - [12] B.-Y. Wang, J.-Y. Hong, K.-H. O. Yang, Y.-L. Chan, D.-H. Wei, H.-J. Lin, and M.-T. Lin, *Phys. Rev. Lett.* **110**, 117203 (2013).
  - [13] J. Wu, J. Choi, A. Scholl, A. Doran, E. Arenholz, C. Hwang, and Z. Q. Qiu, *Phys. Rev. B* **79**, 212411 (2009).
  - [14] J. Wu, J. S. Park, W. Kim, E. Arenholz, M. Liberati, A. Scholl, Y. Z. Wu, C. Hwang, and Z. Q. Qiu, *Phys. Rev. Lett.* **104**, 217204 (2010).
  - [15] J. Li, Y. Meng, J. S. Park, C. A. Jenkins, E. Arenholz, A. Scholl, A. Tan, H. Son, H. W. Zhao, C. Hwang, Y. Z. Wu, and Z. Q. Qiu, *Phys. Rev. B* **84**, 094447 (2011).

- [16] J. Li, A. Tan, S. Ma, R. F. Yang, E. Arenholz, C. Hwang, and Z. Q. Qiu, *Phys. Rev. Lett.* **113**, 147207 (2014).
- [17] R. Morales, Z.-P. Li, J. Olamit, K. Liu, J. M. Alameda, and I. K. Schuller, *Phys. Rev. Lett.* **102**, 097201 (2009).
- [18] Q. Li, T. Gu, J. Zhu, Z. Ding, J. X. Li, J. H. Liang, Y. M. Luo, Z. Hu, C. Y. Hua, H.-J. Lin, T. W. Pi, C. Won, and Y. Z. Wu, *Phys. Rev. B* **91**, 104424 (2015).
- [19] Q. Li, G. Chen, T. P. Ma, J. Zhu, A. T. N'Diaye, L. Sun, T. Gu, Y. Huo, J. H. Liang, R. W. Li, C. Won, H. F. Ding, Z. Q. Qiu, and Y. Z. Wu, *Phys. Rev. B* **91**, 134428 (2015).
- [20] T. Ambrose and C. L. Chien, *Phys. Rev. Lett.* **76**, 1743 (1996).
- [21] P. Kuświk, P. L. Gastelois, M. M. Soares, H. C. N. Tolentino, M. De Santis, A. Y. Ramos, A. D. Lamirand, M. Przybylski, and J. Kirschner, *Phys. Rev. B* **91**, 134413 (2015).
- [22] J. Li, M. Przybylski, F. Yildiz, X. L. Fu, and Y. Z. Wu, *Phys. Rev. B* **83**, 094436 (2011).
- [23] T. J. Moran, J. Nogués, D. Lederman, and I. K. Schuller, *Appl. Phys. Lett.* **72**, 617 (1998).
- [24] D. Alders, L. H. Tjeng, F. C. Voogt, T. Hibma, G. A. Sawatzky, C. T. Chen, J. Vogel, M. Sacchi, and S. Iacobucci, *Phys. Rev. B* **57**, 11623 (1998).
- [25] M. W. Haverkort, S. I. Csiszar, Z. Hu, S. Altieri, A. Tanaka, H. H. Hsieh, H.-J. Lin, C. T. Chen, T. Hibma, and L. H. Tjeng, *Phys. Rev. B* **69**, 020408(R) (2004).
- [26] W. N. Cao, J. Li, G. Chen, J. Zhu, C. R. Hu, and Y. Z. Wu, *Appl. Phys. Lett.* **98**, 262506 (2011).
- [27] S. I. Csiszar, M. W. Haverkort, Z. Hu, A. Tanaka, H. H. Hsieh, H.-J. Lin, C. T. Chen, T. Hibma, and L. H. Tjeng, *Phys. Rev. Lett.* **95**, 187205 (2005).
- [28] J. Zhu, Q. Li, J. X. Li, Z. Ding, C. Y. Hua, M. J. Huang, H.-J. Lin, Z. Hu, C. Won, and Y. Z. Wu, *J. Appl. Phys.* **115**, 193903 (2014).
- [29] G. van der Laan, E. Arenholz, R. V. Chopdekar, and Y. Suzuki, *Phys. Rev. B* **77**, 064407 (2008).
- [30] Y. Z. Wu, Z. Q. Qiu, Y. Zhao, A. T. Young, E. Arenholz, and B. Sinkovic, *Phys. Rev. B* **74**, 212402 (2006).
- [31] W. Kim, E. Jin, J. Wu, J. Park, E. Arenholz, A. Scholl, C. Hwang, and Z. Q. Qiu, *Phys. Rev. B* **81**, 174416 (2010).
- [32] J. Wu, J. Choi, A. Scholl, A. Doran, E. Arenholz, Y. Z. Wu, C. Won, C. Hwang, and Z. Q. Qiu, *Phys. Rev. B* **80**, 012409 (2009).
- [33] H. Ohldag, A. Scholl, F. Nolting, S. Anders, F. U. Hillebrecht, and J. Stöhr, *Phys. Rev. Lett.* **86**, 2878 (2001).
- [34] K. Lenz, S. Zander, and W. Kuch, *Phys. Rev. Lett.* **98**, 237201 (2007).
- [35] R. Bali, M. M. Soares, A. Y. Ramos, H. C. N. Tolentino, F. Yildiz, C. Boudot, O. Proux, M. De Santis, M. Przybylski, and J. Kirschner, *Appl. Phys. Lett.* **100**, 132403 (2012).
- [36] D. Giannotti, H. Hedayat, G. Vinai, A. Picone, A. Calloni, G. Berti, M. Riva, G. Bussetti, F. Boschini, P. Torelli, G. Panaccione, E. Carpena, C. Dallera, M. Finazzi, and A. Brambilla, *Appl. Phys. Lett.* **109**, 232401 (2016).
- [37] J. Gurgul, E. Młyńczak, A. Kozioł-Rachwał, K. Matlak, K. Freindl, E. Madej, N. Spiridis, T. Ślęzak, and J. Korecki, *Phys. Rev. B* **96**, 104421 (2017).
- [38] M. Pilard, O. Ersen, S. Cherifi, B. Carvello, L. Roiban, B. Muller, F. Scheurer, L. Ranno, and C. Boeglin, *Phys. Rev. B* **76**, 214436 (2007).
- [39] C. Gatel, E. Snoeck, V. Serin, and A. R. Fert, *Eur. Phys. J. B* **45**, 157 (2005).
- [40] P. K. Manna, E. Skoropata, Y.-W. Ting, K.-W. Lin, J. W. Freeland, and J. van Lierop, *J. Phys.: Condens. Matter* **28**, 486004 (2016).
- [41] T. J. Regan, H. Ohldag, C. Stamm, F. Nolting, J. Lüning, J. Stöhr, and R. L. White, *Phys. Rev. B* **64**, 214422 (2001).
- [42] Y. Shim and J. G. Amar, *Phys. Rev. Lett.* **98**, 046103 (2007).
- [43] D. Yi, C. L. Flint, P. P. Balakrishnan, K. Mahalingam, B. Urwin, A. Vailionis, A. T. N'Diaye, P. Shafer, E. Arenholz, Y. Choi, K. H. Stone, J.-H. Chu, B. M. Howe, J. Liu, I. R. Fisher, and Y. Suzuki, *Phys. Rev. Lett.* **119**, 077201 (2017).